Liu et al. *NPG Asia Materials* (2018) 10: 552-561
DOI 10.1038/s41427-018-0055-0

NPG Asia Materials

ARTICLE Open Access

Efficiency and stability enhancement of perovskite solar cells by introducing $CsPbI_3$ quantum dots as an interface engineering layer

Chang Liu[1,2], Manman Hu[1], Xianyong Zhou[1], Jianchang Wu[1], Luozheng Zhang[1], Weiguang Kong[1], Xiangnan Li[1], Xingzhong Zhao[2], Songyuan Dai[3], Baomin Xu[1] and Chun Cheng[1]

Abstract

Although great efforts have been devoted to enhancing the efficiency and stability of perovskite solar cells (PSCs), the performance of PSCs has been far lower than anticipated. Interface engineering is helpful for obtaining high efficiency and stability through control of the interfacial charge transfer in PSCs. This paper demonstrates that the efficiency and stability of PSCs can be enhanced by introducing stable α-$CsPbI_3$ quantum dots (QDs) as an interface layer between the perovskite film and the hole transport material (HTM) layer. By synergistically controlling the valence band position (VBP) of the perovskite and the interface layer, an interface engineering strategy was successfully used to increase the efficiency of hole transfer from the perovskite to the HTM layer, resulting in the power conversion efficiency increasing from 15.17 to 18.56%. In addition, the enhancement of the stability of PSCs can be attributed to coating inorganic $CsPbI_3$ QDs onto the perovskite layer, which have a high moisture stability and result in long-term stability of the PSCs in ambient air.

Introduction

Research to achieve high-efficiency solar cells is currently very active[1,2]. As one of the most quickly developing solar cells, perovskite solar cells (PSCs) have become a hot research topic because of their high solar conversion efficiencies and low cost[3–5]. PSCs have made impressive progress in just a few years with record power conversion efficiencies (PCEs) evolving from 3.8% in 2009 to a certified 22.1% in 2016 [6–10]. However, the development of PSCs is still restricted by the instability of the organic composition of PSCs in the presence of water and ambient moisture. To improve the stability of PSC devices, some recent papers have reported that composition engineering by doping with cations is effective for obtaining intrinsically stable perovskites with good properties. Seok et al. first found that the mixed type $(FAPbI_3)_{0.85}(MAPbBr_3)_{0.15}$ perovskite exhibits an excellent efficiency and stability[11]. Inorganic cations have also been incorporated into multiple cation perovskites, such as Cs^+ and Rb^+, to improve the stability of PSC devices[12,13]. Although remarkable progress has been achieved, the crystal structure and energy band compatibility of the materials have largely hindered further improvement using this mixed perovskite strategy. Recently, another effective strategy was reported for promoting the stability of PSCs, i.e., coating barrier layers on the surface of the perovskite layer, and this strategy has been shown to be effective for improving device stability in ambient air[14]. Yang et al. utilized hydrophobic ammonium ions to modify the surface of a perovskite layer and improved the moisture stability[15]. Wang et al. utilized a hydrophobic

Correspondence: Baomin Xu (xubm@sustc.edu.cn) or Chun Cheng (chengc@sustc.edu.cn)
[1]Department of Materials Science and Engineering, Southern University of Science and Technology, 518055 Shenzhen, Guangdong Province, China
[2]Department of Physics, Wuhan University, 430072 Wuhan, Hubei Province, China
Full list of author information is available at the end of the article.
These authors contributed equally: Chang Liu, Manman Hu.

fluorosilane layer as a water-resistant layer, resulting in greater stability of the perovskite film in water[16]. Nevertheless, these studies have ignored the band position matching factor (BPMF) between the barrier layer and the perovskite layer. On the other hand, a large number of studies have demonstrated that the BPMF greatly affects the charge transport efficiencies (CTEs) between the perovskite layer and the interface layer, which can substantially change the PCEs of PSCs[17–19]. These results inspire us to design a new interface engineering layer to improve both the stability and efficiency of PSCs at the same time. To achieve this strategy, the interface engineering layer should possess two important properties, a suitable band position and high moisture resistance. Unfortunately, until now, few materials have been recorded to possess these two properties.

Recently, all-inorganic perovskite materials have exhibited better environmental durability than organic −inorganic hybrid perovskite materials[20]. Furthermore, the band position of inorganic perovskite quantum dot (QD) materials is tunable by adjusting the components of the QDs[21]. However, it is difficult to deposit a dense and uniform QD film. Therefore, to date, it is still a challenge to achieve high PCEs with PSCs fabricated using inorganic perovskite materials as the light-absorption layer[22]. Considering their advantages and disadvantages, we believe that inorganic perovskite QDs are appropriate for use as an interface engineering layer in PSCs due to their superior stability and tunable band gap position.

Among all-inorganic perovskite materials, cubic $CsPbI_3$ may be the most appropriate candidate as an interface engineering material due to its high valence band position (VBP) and high moisture stability. In addition, the synthesis of $CsPbI_3$ QDs can effectively improve the stability of the cubic phase due to the generous contribution of the surface energy[23]. In this work, we propose an interface engineering method to enhance both the efficiency and stability of PSCs by introducing stable $CsPbI_3$ QDs between the perovskite layer and the hole-transporting material (HTM) layer. Furthermore, we used mixed-type perovskite $MA_{0.17}FA_{0.83}Pb(I_{0.83}Br_{0.17})_3$ (marked as FAMAPbI$_3$) as the light-absorption layer to further fulfill the VBP matching requirement between the perovskite layer and the $CsPbI_3$ QD layer. Our results demonstrated that PSCs containing $CsPbI_3$ QDs have a much higher PCE and better stability in ambient air than those without $CsPbI_3$ QDs. The results indicate that this is a new strategy to achieve both high efficiency and stable PSCs by utilizing inorganic perovskite QDs.

Experimental procedures

Materials

Mesoporous TiO_2 paste (Dyesol), formamidinium iodide (FAI), lead iodide (PbI_2), methylammonium bromide (MABr) and lead bromide ($PbBr_2$) were purchased from Xi'an Polymer Light Technology Corp. 2,2′,7,7′-Tetrakis(*N*,*N*-di-p-methoxyphenylamine)-9,9′-spirobifluorene (Spiro-OMeTAD) was purchased from Feiming Chemical Limited. Cesium carbonate (Cs_2CO_3) was purchased from Aladdin. Lead iodide (PbI_2, 99.9985%) was purchased from Alfa Aesar. All the other salts and anhydrous solvents were purchased from Sigma-Aldrich, including oleic acid (OA), oleylamine (OAm), 1-octadecene (ODE), hexane, octane, methyl acetate (MeOAc), lithium *bis*[(trifluoromethyl) sulfonyl] imide salt (Li-TFSI), titanium diisopropoxide *bis* (acetylacetonate) (75 wt% in isopropyl alcohol), *N*,*N*-dimethylformamide (DMF), ethanol, isopropyl alcohol, tert-butylpyridine (tBP), chlorobenzene, acetonitrile, 1-butanol, and dimethyl sulfoxide (DMSO). All the above chemical products were used directly without further purification or other treatment.

Synthesis of Cs-oleate as a cesium precursor

First, 0.2 g (0.614 mmol) of Cs_2CO_3, 0.8 ml of OA and 20 ml of ODE were mixed in a 100 ml three-necked round bottom flask and magnetically stirred under vacuum for 30 min at 120 °C. The mixture was then purged with N_2 for 10 min and placed back under vacuum. This process of alternating vacuum and N_2 was repeated three times to remove the reaction moisture and O_2 until the solution was clear, which indicated that Cs_2CO_3 had reacted with the OA completely. The Cs-oleate solution was stored in N_2 at 70 °C before use.

Synthesis of colloidal $CsPbX_3$ (X = I, Br) QDs

First, 50 ml of ODE and 2.168 mmol PbX_2, i.e., 1 g PbI_2 and 0.8 g $PbBr_2$, were placed in a 500 ml three-necked round bottom flask and heated to 120 °C under vacuum for 1 h with stirring. Then, 5 ml each of OA and OAm were pre-heated to 70 °C and then added to the flask under N_2. The reaction solution was put under vacuum at 120 °C for 30 min until all the PbX_2 dissolved. Then, the temperature was raised to 170 °C under vacuum for 10 min. Next, 8 ml of the as-synthesized Cs-oleate solution, which was pre-heated at 70 °C, was quickly injected into the reaction mixture. After 5~10 s, the flask was submersed in an ice bath to quench the reaction.

Purification

The crude solution of $CsPbX_3$ was precipitated by adding 200 ml of methyl acetate and then centrifuged at 8000 rpm for 5 min. Next, the supernatant was discarded, and the precipitate was dispersed in 3 ml of hexane, precipitated again by adding an equal volume of MeOAc, and centrifuged at 8000 rpm for 5 min. The precipitate was redispersed in 20 ml of hexane and centrifuged at 8000 rpm for 5 min once more. Finally, the supernatant

solution was kept in a freezer for 48 h. The colloidal $CsPbX_3$ solution was decanted and centrifuged at 8000 rpm for 5 min before use. The as-prepared QDs were stored in octane and dispersed in chlorobenzene at a concentration of 20 mg/ml before deposition.

Device fabrication

Fluorine-doped tin oxide (FTO) glasses (Nippon Sheet Glass) were cleaned with detergent, deionized water, and acetone and sonicated with ethanol in an ultrasonic bath for 30 min. Then, the FTO glasses were treated in a UV cleaner for 30 min. The cleaned FTO glasses were coated with 0.15 M titanium diisopropoxide *bis*(acetylacetonate) in a 1-butanol solution by a spin-coating method at 2000 rpm for 60 s, followed by heating at 125 °C for 5 min. The films were cooled to room temperature, and a 0.15 M titanium diisopropoxide *bis*(acetylacetonate) solution in 1-butanol was spin coated on the glasses again to create a pin hole-free dense TiO_2 film. Then, the substrates were calcined in a box furnace at 450 °C for 30 min. The mesoporous TiO_2 (mp-TiO_2) layer was deposited on the dense TiO_2 layer by spin coating a TiO_2 ethanol solution containing 14.3 wt % TiO_2 paste at 4000 rpm for 20 s, and the glass was then calcined at 500 °C for 0.5 h. The precursor solution of the mixed perovskite consisted of 172 mg FAI, 507 mg PbI_2, 22.4 mg MABr and 73.4 mg $PbBr_2$ dissolved in 1 ml of a mixed solvent of DMF and DMSO with a volume ratio of 9:1. The perovskite films were deposited onto the TiO_2 substrates with a two-step spin-coating procedure. The first step was 1000 rpm for 10 s with an acceleration of 500 rpm/s. The second step was 4000 rpm for 35 s with a ramp-up of 2000 rpm/s. Chlorobenzene (~100 µl) was quickly dropped on the spinning substrate during the second spin-coating step 15 s before the end of the procedure. Afterward, the as-prepared films were heated at 100 °C for approximately 2 h until the color changed to dark red. After the substrate was cooled to room temperature, the $CsPbX_3$ QDs dispersed in chlorobenzene (20 mg/ml) were spin coated onto the above $FAMAPbI_3$ perovskite layer at 2000 rpm for 30 s followed by annealing at 90 °C for 2 min. The hole-transporting layer was prepared by spin coating an HTM solution, which was prepared by dissolving Spiro-OMeTAD in chlorobenzene (72.3 mg/ml) with 28.8 µl of a tBP solution and 17.5 µl of Li-*bis*(trifluoromethanesulfonyl) imide lithium salt (Li-TFSI)/acetonitrile (520 mg/ml). The devices were then left overnight in air. Finally, a 100-nm thick Au layer was thermally evaporated under a vacuum of 4×10^{-5} Torr at a rate of ~0.05 nm/s to finish the device fabrication.

Measurement and characterization

UV−Vis absorption spectra were recorded using a Perkin Elmer Lambda 950 UV−Vis-NIR spectrometer. The PL spectra were acquired using a Horiba Fluoromax-4 spectrofluorometer. The time-resolved photoluminescence (TRPL) spectra were collected using a pulse laser as an optical excitation source (A1R FLIM, Nikon). The UPS measurements were performed using an ultraviolet photoelectron spectrometer (ESCALAB 250Xi, Thermo Fisher Scientific) with a He I (21.22 eV) excitation source at an ultrahigh vacuum of 1.0×10^{-10} Torr. X-ray diffraction (XRD) data were collected using a Bruker D8 Discover X-ray diffractometer with Cu Kα radiation (1.54 Å) at 40 kV and 25 mA and a Hi-Star 2D area detector. TEM images were obtained using a Tecnai F30 microscope at 300 kV. The morphology and structure of the films were characterized by field emission scanning electronic microscopy (ZEISS Merlin) at a 5 kV accelerating voltage. The electrochemical impedance spectroscopy (EIS) spectra were recorded by an electrochemical workstation (CHI660, China) in the frequency range of 1 Hz~1 MHz in the dark. Photocurrent density-voltage ($J-V$) curves were measured under AM 1.5 G one sun illumination (100 mW/cm^2) with a solar simulator (Enlitech SS-F7-3A) equipped with 300 W xenon lamp and a Keithley 2400 source meter. The light intensity was adjusted by an NREL-calibrated Si solar cell. During measurements, the cell was covered with a mask with an aperture of 0.1 cm^2. The external quantum efficiency (EQE) was measured with an EQE system (Enlitech QE-R) containing a xenon lamp, monochromator, Si detector, and dual-channel power meter.

Results and discussion

As mentioned above, nanocrystal surfaces are one of the crucial factors in achieving a stable cubic phase of $CsPbI_3$ at room temperature, which is far below the phase-transition temperature for thin films or bulk materials. Here, in our experiment, we chose a simple synthetic route and purification approach to prepare $CsPbI_3$ QDs, which is one of the best methods to keep cubic phase $CsPbI_3$ QDs stable for months in ambient air and even at cryogenic temperatures. We synthesized cubic $CsPbI_3$ QDs using Cs_2Ac and PbI_2 as the precursors and methyl acetate as the shape regulator. Figure 1a is a typical TEM image of the as-prepared $CsPbI_3$ QDs, clearly showing the cubic morphology of the $CsPbI_3$ QDs. The $CsPbI_3$ QDs exhibit a narrow size distribution range between 9 and 13 nm. The high-resolution transmission electron micrograph (HR-TEM) of the sample synthesized at 170 °C (Fig. 1a inset) shows an interplanar distance of 0.31 nm, which was calculated from the bright-field imaging and is consistent with the (200) plane of cubic phase $CsPbI_3$. The corresponding normalized PL spectrum of the $CsPbI_3$ QDs is shown in Fig. 1b. The emission peak of $CsPbI_3$ located at 670 nm corresponds to a $CsPbI_3$ QD size close to 13 nm, which is consistent with the results shown in the TEM image[24]. As shown in Fig. 1c, the

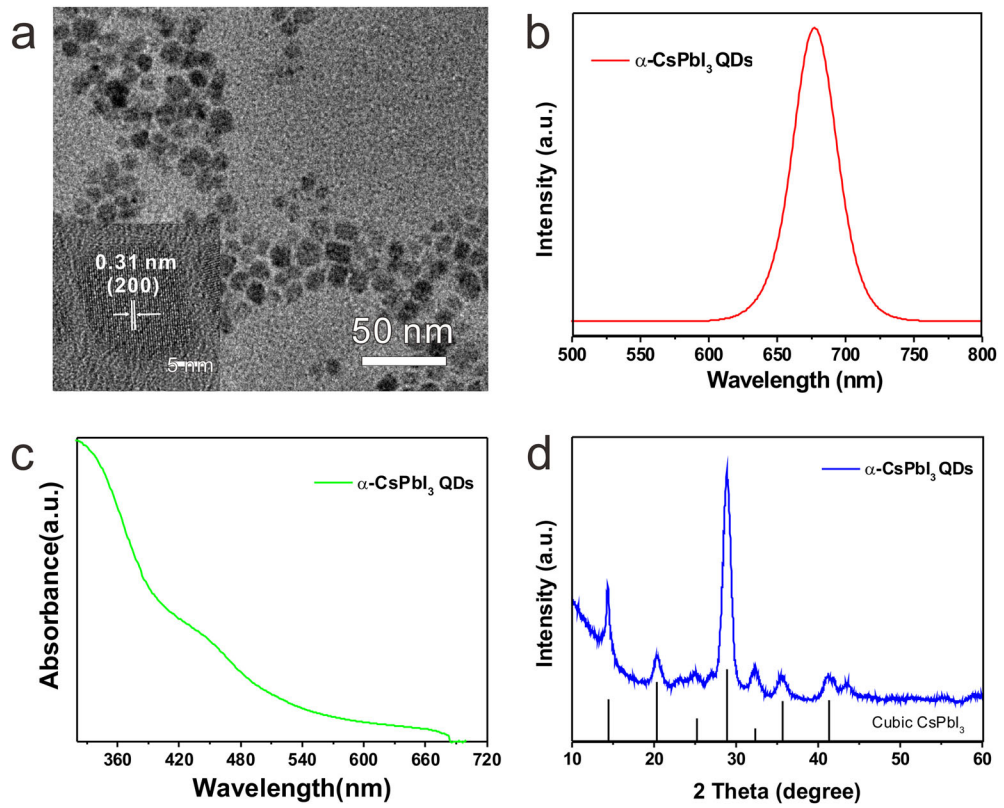

Fig. 1 Properties of $CsPbI_3$ QDs. a TEM and HR-TEM images of $CsPbI_3$ QDs prepared by a simple solution process; **b** photoluminescence spectra; **c** UV—Vis absorption spectra; and **d** powder XRD patterns of the $CsPbI_3$ QDs

UV—Vis absorption spectrum of the $CsPbI_3$ QD solution reveals that the $CsPbI_3$ QDs exhibit a strong absorption in the visible-light region, extending up to 700 nm. Meanwhile, the band gap of α-$CsPbI_3$ QDs between the conduction band (CB) edge and the valence band (VB) edge is determined by the wavelength of the onset of absorption, according to a method in previous literature[25,26]. The value is 1.83 eV for the $CsPbI_3$ QDs. In Fig. 1d, the powder XRD pattern of the $CsPbI_3$ QD film confirms that all the diffraction peaks belong to the cubic phase of $CsPbI_3$, showing no orthorhombic phase formation.

The experimental design for the interface engineering process of PSCs by $CsPbI_3$ QDs is schematically depicted in Fig. 2a. The devices were made by a one-step spin coating of perovskite precursor solutions onto mesoporous TiO_2 (m-TiO_2). PSC devices were fabricated by spin coating QDs onto the surface of the $FAMAPbI_3$ perovskite film and then using the same steps required for the mesoporous $FAMAPbI_3$/HTM structure. Detailed information on the perovskite precursor solution preparation, $CsPbI_3$ QD deposition, and fabrication of the devices is given in the experimental section. The optimal PSC device structure consists of a 30-nm thick compact TiO_2 (c-TiO_2) layer on FTO, a 500-nm thick perovskite layer with mesoporous TiO_2, a 150-nm thick Spiro-OMeTAD layer as the HTM layer, and a thermally evaporated Au layer (100 nm) as the back contact, as shown in the cross-sectional scanning electron microscopy (SEM) image in Fig. 2b. It should be noted that both HTM and $CsPbI_3$ QD layers were processed from CB. To examine the effect of HTM processing for the $CsPbI_3$ QD layer, the pure CB was spin-coated on the surface of $CsPbI_3$ QD layer with same experimental condition. As shown in Fig. S1, the $CsPbI_3$ QD layers show no obvious change after coating CB, indicating that the deposition of CB did not affect the $CsPbI_3$ QD layer. The synthesized $CsPbI_3$ QDs were deposited as an interface engineering layer between the $FAMAPbI_3$ perovskite film and the HTM layer, and an $FAMAPbI_3$/$CsPbI_3$ QDs/HTM device structure (Fig. 2e) was proposed and investigated in this work. Comparing the cross-sectional SEM images of the PSC devices without and with QDs, it is difficult to observe an obvious boundary between the $CsPbI_3$ QD layer and HTM. Therefore, to determine the thickness of the $CsPbI_3$ QD layer, an atomic force microscopy (AFM) test of a single $CsPbI_3$ QD layer deposited on a Si surface (Fig. S2) and cross-sectional SEM images of PSC devices without an HTM (Fig. S3) were processed. The thickness

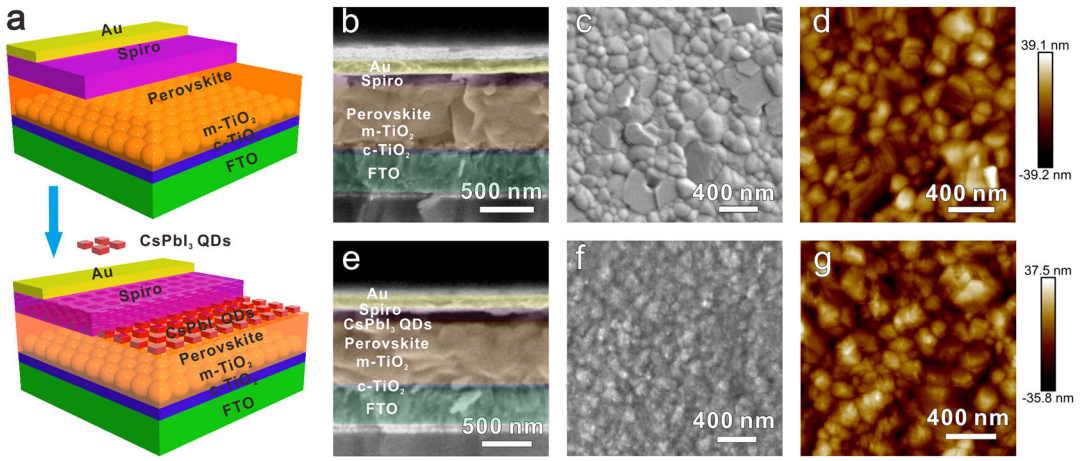

Fig. 2 Structure and morphology of PSCs with and without $CsPbI_3$ QD. a Schematic diagram showing the fabrication process of $CsPbI_3$ QD interface engineering. **b**, **e** SEM cross-section of perovskite solar cells without and with $CsPbI_3$ QD deposition. **c**, **f** Top-view SEM images of the perovskite layer before and after deposition of $CsPbI_3$ QDs. **d**, **g** AFM images of the perovskite film without and with $CsPbI_3$ QD deposition

of the $CsPbI_3$ QD layer calculated from these characterizations is ~30 nm. The formation of the $CsPbI_3$ QD layer can be further verified from the top-view SEM images of the perovskite film before and after deposition of the $CsPbI_3$ QDs, which are shown in Fig. 2c, f, respectively. After depositing the $CsPbI_3$ QDs, both the top-view and cross-sectional SEM images (Fig. S3) confirm that the $CsPbI_3$ QDs were relatively homogenously deposited on the surface of the $FAMAPbI_3$ film. The impact of the number of spin coatings and the concentration of the $CsPbI_3$ QDs on the performance of the PSCs was investigated. The amount of $CsPbI_3$ QDs deposited onto the $FAMAPbI_3$ perovskite film was tuned by changing the concentration of the $CsPbI_3$ QD suspension and by varying the number of spin coatings. Qualitatively, the amount of $CsPbI_3$ QDs significantly influences the photovoltaic performance. Spin coating a 20 mg/ml $CsPbI_3$ QD solution produced the best performance in our experiments. All PSC devices interfaced with the perovskite QDs in this work were fabricated under these optimized conditions. It can be speculated that the deposited $CsPbI_3$ QDs penetrate the remaining, available perovskite pore volume, leading to a smoother top capping layer on the perovskite film. To demonstrate this assumption, we performed an AFM measurement to examine the surface roughness of a perovskite film surface in a 2 μm × 2 μm area. The typical AFM topography of a perovskite film without $CsPbI_3$ QD deposition is illustrated in Fig. 2d. The grain size observed in the AFM image is consistent with that observed in the SEM image in Fig. 2c. Additionally, the AFM image shows a similar root mean square roughness value of 11.1 nm, which ranges from 9.5 to 13.9 nm, as shown in Fig. S4. As shown in Fig. 2g, after the $CsPbI_3$ QD deposition, the roughness of the perovskite dramatically decreased to 7.01 nm and ranged from 5.5 to 8.4 nm (Fig. S4), indicating a promising effect of $CsPbI_3$ QDs with respect to morphological control of perovskite thin films.

It is well known that due to higher HOMO level, the deposition of Spiro-OMeTAD on the surface of a perovskite layer will lend to the transfer of holes from the perovskite layer to Spiro, but the high energy gap between the perovskite layer and Spiro leads to high voltage loss and a low hole transfer rate[27,28]. Therefore, interface engineering by inserting $CsPbI_3$ QDs with a VBP located between the VB of the $FAMAPbI_3$ perovskite and the HOMO of the HTM can facilitate hole transfer at the interface, reducing recombination between photogenerated electrons and holes during the transport process. To confirm this idea, we investigated the influence of the $CsPbI_3$ QD deposition on the surface of the $FAMAPbI_3$ layer on the efficiency of the PSCs. The current−voltage ($J-V$) curves for the best PSC devices with and without $CsPbI_3$ QDs are presented in Fig. 3a. Upon introduction of the $CsPbI_3$ QDs, the photovoltaic performance changed dramatically. The best PSC without QDs ($FAMAPbI_3$/HTM) produced an open-circuit voltage (V_{oc}) of 1.049 V, a short-circuit photocurrent density (J_{sc}) of 20.94 mA/cm^2,and a fill factor (FF) of 0.69, corresponding to a PCE of 15.17%. The introduction of $CsPbI_3$ QDs at the $FAMAPbI_3$−HTM interface increased the PCE remarkably to 18.56% because of significant increases in the V_{oc} (1.092 V) and J_{sc} (24.42 mA/cm^2) compared to those of the PSC without QDs. To obtain high V_{oc}, a high charge mobility is important as well as the suitable energy level alignment. The mobility for the $CsPbI_3$ QD film has been reported to be 0.23 cm^2/V/s,which is over 100 times higher than that of

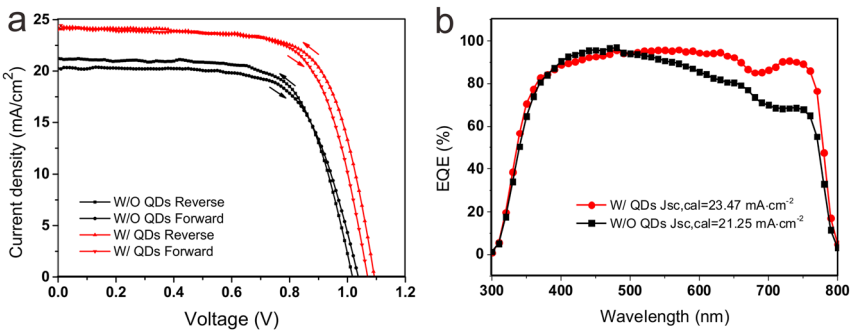

Fig. 3 Device performance of perovskite solar cells. a Typical *J–V* characteristics and **b** corresponding EQE of solar cells W/ $CsPbI_3$ QDs and W/O $CsPbI_3$ QDs

Spiro-OMeTAD (1.80×10^{-3} $cm^2/V/s$)[29]. Hence, the CTE of PSC device could be significantly enhanced by the $CsPbI_3$ QDs deposition thus leading to the high V_{oc}. We also investigated the hysteresis effect in the $J-V$ measurements of the device. As shown in Fig. 3a, the device shows a negligible hysteresis effect under the scan direction. The high-quality PSCs favor highly efficient charge collection, resulting in hysteresis-free PSCs. The certified efficiency of the PSC with $CsPbI_3$ QDs for a 0.1/cm^2 area is 17.30% (Fig. S5). The photovoltaic metrics for 20 devices are shown in Fig. S6. Figure 3b shows the corresponding incident photon-to-current efficiency (IPCE) spectra for the two PSC devices with and without $CsPbI_3$ QDs. The IPCE of PSCs with $CsPbI_3$ QDs is markedly higher than that without $CsPbI_3$ QDs, and the integrated photocurrent densities are 23.47 and 21.25 mA/cm^2 for PSCs with and without $CsPbI_3$ QDs, respectively, which is in agreement with the JSC values derived from the *J–V* measurements. These results indicate that the introduction of $CsPbI_3$ QDs with a suitable VBP at the FAMAPbI$_3$−HTM interface improves the IPCE compared to that of the PSC without $CsPbI_3$ QDs, which meets our expectation.

To our knowledge, additional factors may influence the photovoltaic performance of PSCs. For instance, photocurrent generation is a direct result of the light-harvesting efficiency. The fluorescence from $CsPbI_3$ QDs may enhance light harvesting by the active layer because the emitted photons can be absorbed by the perovskite film. To validate the effectiveness of the $CsPbI_3$ QD interface engineering strategy used, several different experiments were systematically evaluated. As shown in Fig. 4a, the perovskite films with $CsPbI_3$ QDs exhibited slightly enhanced light absorption compared to that without $CsPbI_3$ QDs, especially in the range from 500 to 700 nm. To further study this reason, we measured the light absorption of bare $CsPbI_3$ QDs film and it is found that the $CsPbI_3$ QDs film showed weak light absorption in the range from 500 to 700 nm which is consistent with the above result. Furthermore, the strongly asymmetric enhancement in the EQE spectrum from 500 to 700 nm for PSC with $CsPbI_3$ QDs can be explained by the increased light absorption of $CsPbI_3$ QDs. Because the light-harvesting efficiency of the films is enhanced by the $CsPbI_3$ QDs deposition, the observed difference in performance could attribute to the more effective charge transfer resulted from the $CsPbI_3$ QDs interface engineering as well as the increased light absorption of the whole PSC device. This mechanism can be further demonstrated by the results from the PL spectra and time-resolved PL decay curves of the perovskite films without and with $CsPbI_3$ QD deposition. The notion inferred above that charge transfer is facilitated by the $CsPbI_3$ QD layer is corroborated by the steady-state PL measurements[30]. Figure 4b shows the steady-state PL spectra of the perovskite films without and with $CsPbI_3$ QDs. Under the same experimental conditions, both perovskite films without and with $CsPbI_3$ QDs exhibit a PL peak at 780 nm. The PL quantum yield of the perovskite film with $CsPbI_3$ QDs is largely reduced compared to that of the film without $CsPbI_3$ QDs, indicating the significantly enhanced charge carrier extraction arises from the addition of the $CsPbI_3$ QDs. Here, $CsPbI_3$ can play a role as a hole acceptor and enhances the charge injection from the perovskite to the HTM layer due to its suitable VBP (slightly higher than that of the perovskite film). To further confirm our speculation, we performed TRPL measurements to study the hole-extraction kinetics at the perovskite−HTM interface[31]. As shown in Fig. 4c, the PL decay lifetime of the perovskite film with $CsPbI_3$ QDs was determined to be 11.13 ns compared to 13.24 ns for the film without $CsPbI_3$ QDs. The PL in the perovskite/$CsPbI_3$ QDs/HTM film shows significant, faster decay than that in the pristine perovskite/HTM film, indicating fast charge transfer from the perovskite into the HTM. These results indicate that perovskite films with $CsPbI_3$ QDs can extract and transport holes more efficiently than those without $CsPbI_3$ QDs, which is

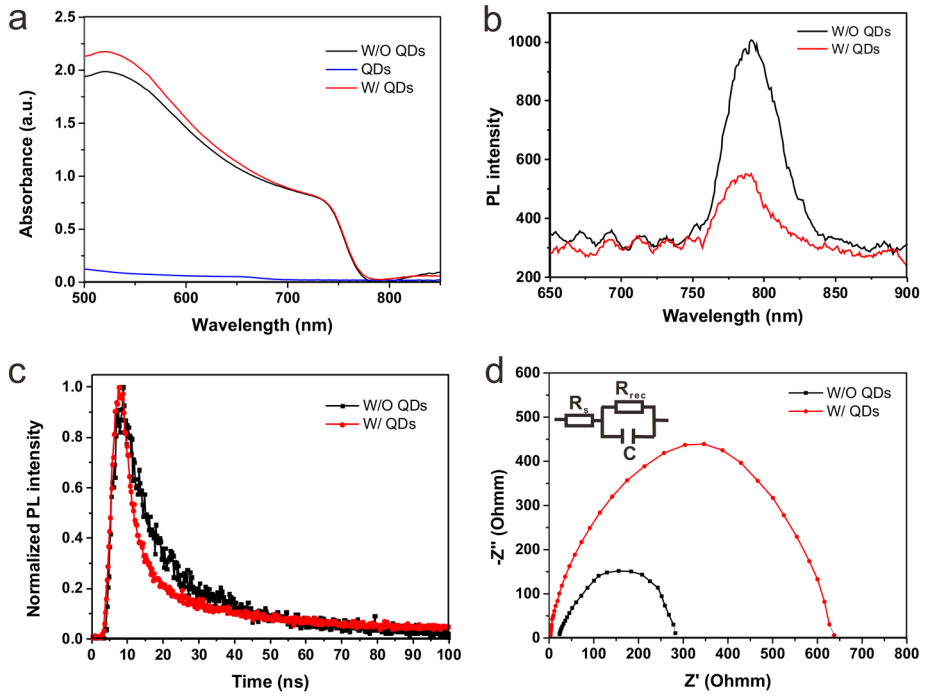

Fig. 4 Light absorption and charge transport properties of PSCs. a UV−Vis absorption spectra of $CsPbI_3$ QD film, perovskite films W/O and W/ $CsPbI_3$ QDs. **b** Photoluminescence spectra and **c** Time-resolved photoluminescence decay curves of perovskite films W/O and W/ $CsPbI_3$ QDs. **d** Electrochemical impedance responses of PSC devices W/O and W/ $CsPbI_3$ QDs measured at an open-circuit voltage under dark conditions at a 0.8 V bias

consistent with the higher performances of the PSC devices with $CsPbI_3$ QDs compared to those of the PSC devices without $CsPbI_3$ QDs.

To further clarify the effect of the $CsPbI_3$ QDs, EIS was carried out to study the photogenerated charge recombination processes in the PSCs. Figure 4d shows the Nyquist spectra of PSCs without and with $CsPbI_3$ QDs in the frequency range of 0.4 kHz to 50 kHz at a foreword bias of 0.8 V under dark conditions. The semicircle in the EIS spectra indicates the charge transfer behavior at the interface between the perovskite and HTM[32]. The equivalent circuit is shown in the Fig. 4d inset. The values of R_s for the PSCs with QDs were lower than those for the PSCs without QDs, indicating that the decrease in the series resistance of the PSC was caused by the addition of the $CsPbI_3$ QDs. On the other hand, the value of R_{rec} for the PSC increased greatly when the $CsPbI_3$ QDs were introduced, suggesting that recombination in the device with $CsPbI_3$ QDs was slower than that in the device without $CsPbI_3$ QDs. Both factors are beneficial for improving efficiency, which is consistent with the $J-V$ measurement results.

The interface engineering between the perovskite layer and HTM induced by the $CsPbI_3$ QDs not only remarkably enhanced the photovoltaic performance of the PSCs but also significantly improved the stability of the PSCs in air. As shown in Fig. S7, the (a) PL spectrum, (b) UV−Vis absorption spectrum and (c) XRD pattern of the $CsPbI_3$ QDs did not show obvious changes even after 30 days of storage in ambient air, demonstrating the outstanding moisture stability of the $CsPbI_3$ QDs. Since excellent moisture resistance has been demonstrated in $CsPbI_3$ QDs, PSCs with $CsPbI_3$ QD modification are expected to have good long-term ambient stability. To investigate the stability of the perovskite devices, the photovoltaic performance of the PSCs was measured every 5 days for 35 days. The evolution of the PCE over time is displayed in Fig. 5a. The initial PCE of the PSC without the $CsPbI_3$ QDs was almost entirely lost after 35 days, corresponding to an attenuation of 100%. In contrast, the PSC with the $CsPbI_3$ QDs experienced a PCE drop of 20% (from 100 to 80%) after 35 days. As shown in Fig. 5a inset, the color of the PSC device without $CsPbI_3$ QDs became yellow after storage in ambient air for 35 days, indicating that the perovskite was mostly decomposed. In contrast, the color of the PSC device with $CsPbI_3$ QDs remained brown, demonstrating that the perovskite hardly changed under the same conditions. Thus, compared to that of the PSC without $CsPbI_3$ QDs, the device with the $CsPbI_3$ QDs exhibited better long-term stability in the ambient air at over 30% RH without any encapsulation due to the high moisture resistance of $CsPbI_3$ QDs. The maximum power

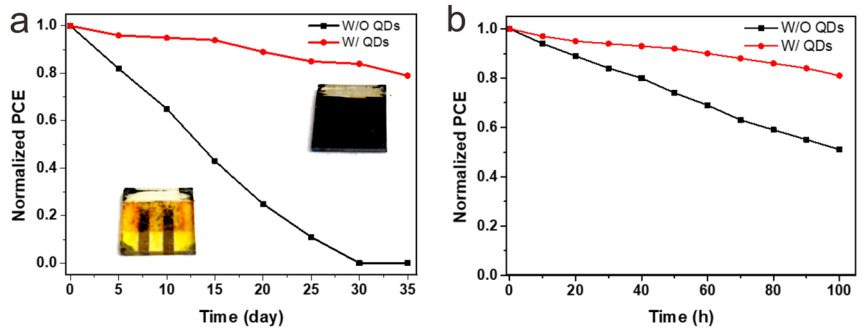

Fig. 5 Performance durability of PSC devices without and with a $CsPbI_3$ QD interface layer. a Dark storage stability of PSCs without and with the $CsPbI_3$ QD interface layer. The insets are digital photos of PSC devices stored in ambient air for 35 days. **b** Normalized performance evolution of the device stored under a nitrogen atmosphere under continuous light irradiation

output (MPO) decay under continuous light illumination is another important technical index for the stability of PSC devices. The PSCs with $CsPbI_3$ QDs showed remarkably enhanced stability under continuous operation at MPO compared to that of the devices without $CsPbI_3$ QDs (Fig. 5b). The PSCs with $CsPbI_3$ QDs retained 81% of their initial performance after continuous operation for 100 h under 1 sun light irradiation. In contrast, the MPO of the PSCs without $CsPbI_3$ QDs declined to 50% under the same conditions, which indicates that the stability of the PSC device can be remarkably enhanced with the addition of the $CsPbI_3$ QD layer. As an all-inorganic perovskite material, $CsPbI_3$ has been demonstrated to exhibit a high stability in ambient air. Therefore, the formation of an interface layer composed of $CsPbI_3$ QDs on the surface of a perovskite film layer may act as a moisture protection layer, enhancing the stability of PSC devices.

The experimental results presented above clearly show that PSCs with $CsPbI_3$ QDs exhibit both a higher photoelectric efficiency and better stability, as we expected. The high photovoltaic efficiency of PSCs with $CsPbI_3$ QDs can be ascribed to their matched energy levels and high hole transfer efficiencies. To further support this idea, we systematically investigated the influence of the VBP on interface engineering materials for PSC devices. The $CsPbBr_3$ QDs with lower VBP than the perovskite film were introduced as an interface layer onto the surface of the perovskite film. As shown in Fig. S8b and d, the successful synthesis of $CsPbBr_3$ QDs was confirmed by the typical PL spectrum and XRD pattern of $CsPbBr_3$. It should be noted that the $CsPbBr_3$ QDs were synthesized by a method similar to that of the $CsPbI_3$ QDs, and the sizes of the two types of QDs were in the same range (Fig. S8a). First, to determine the energy levels of the perovskite, $CsPbI_3$ QDs and $CsPbBr_3$ QDs, UV−Vis absorption spectroscopy and UV photoelectron spectroscopy (UPS) experiments were performed. Figure 6a shows the UPS spectra of the perovskite, $CsPbI_3$ QD and $CsPbBr_3$ QD films. The photoemission parameters obtained from the UPS measurements are summarized in Table S1. The VBP values measured by UPS are −5.60, −5.33, and −5.85 eV for the perovskite, $CsPbI_3$ QD, and $CsPbBr_3$ QD films, respectively. As determined by UV −Vis absorption spectroscopy (Fig. S8c), the band gaps for the three films (perovskite, $CsPbI_3$ QDs, and $CsPbBr_3$ QDs) are 1.62, 1.83, and 2.40 eV, corresponding to −3.98, −3.50, and −3.45 eV CBP values for these films, respectively. Based on these results, the corresponding schematic energy level diagram of the perovskite/interface layer/HTM is displayed in Fig. 6b. Figure 6b illustrates the transfer of photogenerated electrons and holes when $CsPbI_3$ QDs and $CsPbBr_3$ QDs are inserted at the interface between the perovskite layer and HTM, respectively. The $CsPbBr_3$ QDs have a much lower VB edge than the $FAMAPbI_3$ perovskite, which hinders hole transfer from the perovskite film to the HTM layer. In contrast, because the VBP of $CsPbI_3$ QDs is located between that of the HTM and the perovskite, more favorable energy-level alignment occurs at the interface, facilitating cascade hole extraction[33,34]. To further investigate the role of interface engineering in influencing the performance of the fabricated PSC devices, the PL spectra of perovskites without QDs, with $CsPbI_3$ QDs and with $CsPbBr_3$ QDs were measured. As shown in Fig. 6c, the perovskite with $CsPbI_3$ QDs exhibited stronger PL quenching than the perovskite without QDs, while the perovskite with $CsPbBr_3$ QDs exhibited very little PL quenching. The increased PL quenching yield of the perovskite with $CsPbI_3$ QDs indicates improved hole transfer from the perovskite to the HTM. To further validate the effectiveness of the fabrication strategy, the $J-V$ performance of PSC devices without QDs, with $CsPbI_3$ QDs and $CsPbBr_3$ QDs was measured in the study. As shown in Fig. 6d, the $J-V$ tests for PSCs without QDs, with $CsPbI_3$ QDs, and with $CsPbBr_3$ QDs were systematically evaluated, and the

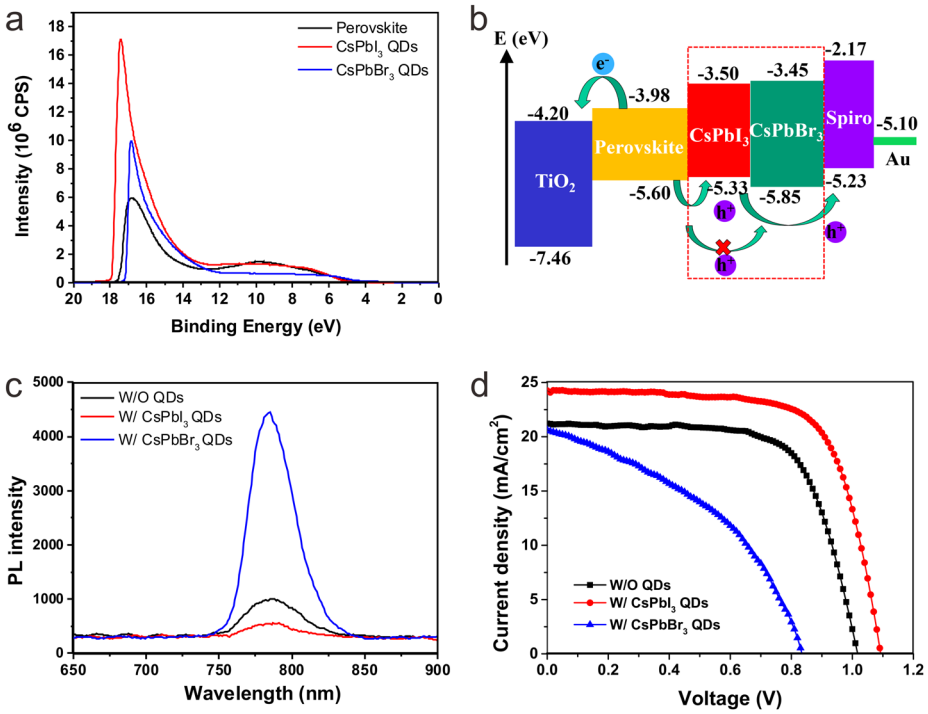

Fig. 6 Band structure properties and device performance of PSCs with different QDs. a UV photoelectron spectroscopy (UPS) results of the perovskite film, $CsPbI_3$ and $CsPbBr_3$ QDs. UPS measurements were performed in an ultra-high vacuum chamber with a He(I) (21.2 eV) discharge lamp. **b** Energy diagrams of each material in the perovskite solar cell device with energy levels in eV. **c** Photoluminescence spectra of perovskite films without QDs and with $CsPbI_3$ QDs or $CsPbBr_3$ QDs. **d** *J*–*V* curves of the best-performing PSC devices without QDs and with $CsPbI_3$ QDs or $CsPbBr_3$ QDs as the interface-regulating material

photovoltaic performance parameters are summarized in Table S2. The average data for 20 PSC devices without QDs prepared under the same conditions were a V_{oc} of 1.02 V, J_{sc} of 22.22 mA/cm^2, and FF of 0.67, corresponding to a PCE of 15.14%. However, interface modification using $CsPbBr_3$ QDs reduced the PCE significantly to 9.45% because of the significant decreases in the V_{oc}, J_{sc} and FF values compared to those of the PSC without QDs. The lower-lying VBP of $CsPbBr_3$ compared to the VB of the perovskite results in a hole-transfer hindering effect, leading to significant decreases in the V_{oc}, FF, and PCE values. In contrast, if the $CsPbBr_3$ QDs were replaced with $CsPbI_3$ QDs, the solar cell device produced a V_{oc} of 1.05 V, J_{sc} of 24.28 mA/cm^2, and FF of 0.71, corresponding to a PCE of 18.14%. The enhancement in the PCE is attributed to the significant improvement in the J_{sc} and FF values as well as the slight increase in V_{oc}. The VBP of the $CsPbI_3$ QDs is located between the VB edge of the perovskite film and the HOMO of the HTM. In this situation, the photogenerated holes in the perovskite film produced by irradiation may first transfer to the $CsPbI_3$ QDs and then to the HTM layer. As a result of the better matching of energy levels among the perovskite, $CsPbI_3$ QDs, and HTM, the two-step hole transfer resulting from such interface engineering facilitates the hole transfer from the perovskite film to the HTM layer[35]. As a consequence, the J_{sc}, V_{oc} and FF values all are enhanced, leading to a significant improvement in the PCE. Our results demonstrated that $CsPbI_3$ QD interface engineering was beneficial to PCE enhancement of PSCs, while the addition of $CsPbBr_3$ QDs had the opposite effect. According to the interface modification design, a suitable VBP is the key factor to improve charge transfer between the perovskite layer and HTM.

Conclusions

We successfully fabricated novel PSCs by introducing $CsPbI_3$ QDs as interface engineering materials. The charge-transfer efficiency at the interface of the perovskite/HTM layer is enhanced by $CsPbI_3$ QDs due to their intermediate VB position between the perovskite and HTM layers. The cascade energy level structure created by interfacial engineering of the $CsPbI_3$ QDs can remarkably improve the hole extraction and the FF, J_{sc}, and PCE values of PSC devices. With this strategy, the PCE of $CsPbI_3$ QD-modified PSCs was substantially enhanced from 15.17 to 18.56% compared to that without $CsPbI_3$ QD modification. Moreover, PSCs with $CsPbI_3$ QDs maintained 82% of their initial performance for 30 days at over 30% RH without any encapsulation,

suggesting that the stability of the PSCs was also markedly improved due to the high stability of the $CsPbI_3$ QDs. This as-established approach is fundamentally new, universally applicable and practically usable for the enhancement of PSCs, which will possibly result in a new pathway to simultaneously improve both the efficiency and stability of solar cells.

Acknowledgements
This work was supported by National Key Research and Development Project funding from the Ministry of Science and Technology of China (Grants nos. 2016YFA0202400 and 2016YFA0202404), Peacock Team Project funding from the Shenzhen Science and Technology Innovation Committee (Grant no. KQTD20150331101823 70), the Guangdong Natural Science Funds for Distinguished Young Scholars (Grant 2015A030306044), the Guangdong-Hong Kong Joint Innovation Project (Grant no. 2016A050503012), the China Postdoctoral Science Foundation (Grant no. 2016M602347), and startup funding from the Southern University of Science and Technology (Grants nos. 25/Y01256112 and 25/Y01256212).

Author details
[1]Department of Materials Science and Engineering, Southern University of Science and Technology, 518055 Shenzhen, Guangdong Province, China. [2]Department of Physics, Wuhan University, 430072 Wuhan, Hubei Province, China. [3]Beijing Key Laboratory of Thin Film Solar Cells, North China Electric Power University, 102206 Beijing, China

Conflict of interest
The authors declare that they have no conflict of interest.

Supplementary information is available for this paper at https://doi.org/10.1038/s41427-018-0055-0.

Received: 9 September 2017 Revised: 5 April 2018 Accepted: 30 April 2018.
Published online: 18 June 2018

References

1. Oregan, B. & Gratzel, M. A low-cost, high-efficiency solar-cell based on dye-sensitized colloidal TiO2 films. *Nature* **353**, 737–740 (1991).
2. Li, G. et al. High-efficiency solution processable polymer photovoltaic cells by self-organization of polymer blends. *Nat. Mater.* **4**, 864–868 (2005).
3. Burschka, J. et al. Sequential deposition as a route to high-performance Perovskite-sensitized solar cells. *Nature* **499**, 316–319 (2013).
4. Lee, M. M., Teuscher, J., Miyasaka, T., Murakami, T. N. & Snaith, H. J. Efficient hybrid solar cells based on meso-superstructured organometal halide perovskites. *Science* **338**, 643–647 (2012).
5. Liu, M., Johnston, M. B. & Snaith, H. J. Efficient planar heterojunction perovskite solar cells by vapour deposition. *Nature* **501**, 395–398 (2013).
6. Kojima, A., Teshima, K., Shirai, Y. & Miyasaka, T. Organometal halide perovskites as visible-light sensitizers for photovoltaic cells. *J. Am. Chem. Soc.* **131**, 6050–6051 (2009).
7. Xing, G. et al. Long-range balanced electron- and hole-transport lengths in organic−inorganic Ch3nh3pbi3. *Science* **342**, 344–347 (2013).
8. Yang, W. S. et al. High-performance photovoltaic perovskite layers fabricated through intramolecular exchange. *Science* **348**, 1234–1237 (2015).
9. Zhou, H. et al. Interface engineering of highly efficient perovskite solar cells. *Science* **345**, 542–546 (2014).
10. Tan, H. et al. Efficient and stable solution-processed planar perovskite solar cells via contact passivation. *Science* **355**, 722–726 (2017).
11. Jeon, N. J. et al. Compositional engineering of perovskite materials for high-performance solar cells. *Nature* **517**, 476–480 (2015).
12. Saliba, M. et al. Cesium-containing triple cation perovskite solar cells: improved stability, reproducibility and high efficiency. *Energy Environ. Sci.* **9**, 1989–1997 (2016).
13. Saliba, M. et al. Incorporation of rubidium cations into perovskite solar cells improves photovoltaic performance. *Science* **354**, 206–209 (2016).
14. Liu, C. et al. Efficient and stable perovskite solar cells prepared in ambient air based on surface-modified perovskite layer. *J. Phys. Chem. C.* **121**, 6546–6553 (2017).
15. Yang, S. et al. Functionalization of perovskite thin films with moisture-tolerant molecules. *Nat. Energy* **1**, 15016 (2016).
16. Wang, Q., Dong, Q., Li, T., Gruverman, A. & Huang, J. Thin insulating tunneling contacts for efficient and water-resistant perovskite solar cells. *Adv. Mater.* **28**, 6734–6739 (2016).
17. Malinkiewicz, O. et al. Metal-oxide-free methylammonium lead iodide perovskite-based solar cells: the influence of organic charge transport layers. *Adv. Energy Mater.* **4**, 1400345 (2014).
18. Malinkiewicz, O. et al. Perovskite solar cells employing organic charge-transport layers. *Nat. Photonics* **8**, 128–132 (2014).
19. Kim, J. et al. Efficient planar-heterojunction perovskite solar cells achieved via interfacial modification of a sol–gel Zno electron collection layer. *J. Mater. Chem. A* **2**, 17291–17296 (2014).
20. Luo, P. et al. Solvent engineering for ambient-air-processed, phase-stable Cspbi3 in perovskite solar cells. *J. Phys. Chem. Lett.* **7**, 3603–3608 (2016).
21. Nedelcu, G. et al. Fast anion-exchange in highly luminescent nanocrystals of cesium lead halide perovskites (Cspbx3, X=Cl, Br, I). *Nano Lett.* **15**, 5635–5640 (2015).
22. Wang, Y. et al. All-inorganic colloidal perovskite quantum dots: a new class of lasing materials with favorable characteristics. *Adv. Mater.* **27**, 7101–7108 (2015).
23. Swarnkar, A. et al. Quantum dot-induced phase stabilization of AlphCsPbI3 perovskite for high-efficiency photovoltaics. *Science* **354**, 92–95 (2016).
24. Zeng, H. et al. Blue luminescence of Zno nanoparticles based on non-equilibrium processes: defect origins and emission controls. *Adv. Funct. Mater.* **20**, 561–572 (2010).
25. Song, J. et al. Quantum dot light-emitting diodes based on inorganic perovskite cesium lead halides (Cspbx3). *Adv. Mater.* **27**, 7162–7167 (2015).
26. Wu, Y. et al. Perovskite solar cells with 18.21% efficiency and area over 1 cm^2 fabricated by heterojunction engineering. *Nat. Energy* **1**, 1614–1618 (2016).
27. Li, C. et al. Efficient perovskite/fullerene planar heterojunction solar cells with enhanced charge extraction and suppressed charge recombination. *Nanoscale* **7**, 9771–9778 (2015).
28. Bi, D. et al. Facile synthesized organic hole transporting material for perovskite solar cell with efficiency of 19.8%. *Nano Energy* **23**, 138–144 (2016).
29. Sanehira, E. M. et al. Enhanced mobility CsPbI3 quantum dot arrays for record-efficiency, high-voltage photovoltaic cells. *Sci. Adv.* **3**, eaao4204 (2017).
30. Docampo, P., Ball, J. M., Darwich, M., Eperon, G. E. & Snaith, H. J. Efficient organometal trihalide perovskite planar-heterojunction solar cells on flexible polymer substrates. *Nat. Commun.* **4**, 2761 (2013).
31. Rakstys, K. et al. Triazatruxene-based hole transporting materials for highly efficient perovskite solar cells. *J. Am. Chem. Soc.* **137**, 16172–16178 (2015).
32. Lv, M. et al. Colloidal Cuins2 quantum dots as inorganic hole-transporting material in perovskite solar cells. *ACS Appl. Mater. Interfaces* **7**, 17482–17488 (2015).
33. Ravi, V. K., Markad, G. B., & Nag, A. Band edge energies and excitonic transition probabilities of colloidal Cspbx3(X = Cl, Br, I) perovskite nanocrystals. *ACS Energ. Lett.* **1**, 665–671 (2010).
34. Lee, Y.-L., Chi, C.-F. & Liau, S.-Y. Cds/Cdse co-sensitized Tio2 photoelectrode for efficient hydrogen generation in a photoelectrochemical cell. *Chem. Mater.* **22**, 922–927 (2009).
35. Yang, D. et al. Hysteresis-suppressed high-efficiency flexible perovskite solar cells using solid-state ionic-liquids for effective electron transport. *Adv. Mater.* **28**, 5206–5213 (2016).